

Accepted for publication in the Astrophysical Journal

# THE LIFETIME OF PROTOPLANETARY DISKS IN A LOW-METALLICITY ENVIRONMENT<sup>1</sup>

Chikako Yasui and Naoto Kobayashi

*Institute of Astronomy, School of Science, University of Tokyo, 2-21-1 Osawa, Mitaka,  
Tokyo 181-0015, Japan*

ck\_yasui@ioa.s.u-tokyo.ac.jp

Alan T. Tokunaga

*Institute for Astronomy, University of Hawaii, 2680 Woodlawn Drive, Honolulu, HI 96822,  
USA*

Masao Saito

*ALMA Project, National Astronomical Observatory of Japan, 2-21-1 Osawa, Mitaka,  
Tokyo 181-8588, Japan*

and

Chihiro Tokoku

*Astronomical Institute, Tohoku University, Aramaki, Aoba, Sendai 980-8578, Japan*

## ABSTRACT

The extreme outer Galaxy (EOG), the region with a Galactic radius of more than 18 kpc, is known to have very low metallicity, about one-tenth that of the solar neighborhood. We obtained deep near-infrared (NIR) images of two very young ( $\sim 0.5$  Myr) star-forming clusters that are one of the most distant embedded clusters in the EOG. We find that in both clusters the fraction of stars with NIR excess, which originates from the circumstellar dust disk at radii of  $\leq 0.1$  AU, is significantly lower than those in the solar neighborhood. Our results suggest that most stars forming in the low-metallicity environment experience disk dispersal at an earlier stage ( $< 1$  Myr) than those forming in the solar metallicity environment (as much as  $\sim 5$ – $6$  Myr). Such rapid disk dispersal may make the

formation of planets difficult, and the shorter disk lifetime with lower metallicity could contribute to the strong metallicity dependence of the well-known “planet-metallicity correlation”, which states the probability of a star hosting a planet increases steeply with stellar metallicity. The reason for the rapid disk dispersal could be increase of the mass accretion rate and/or the effective far-ultraviolet photoevaporation due to the low extinction; however, another unknown mechanism for the EOG environment could be contributing significantly.

*Subject headings:* infrared: stars – planetary systems: protoplanetary disks – stars: pre-main-sequence – open clusters and associations: individual (Digel Cloud 2) – stars: formation

## 1. INTRODUCTION

Because the EOG is known to have an extreme environment such as very low metallicity,  $[O/H] \sim -1$  (Rudolph et al. 2006), it can be studied as a “laboratory” for the star formation process in an environment totally different from the solar neighborhood (Ferguson et al. 1998; Kobayashi et al. 2008). As a part of our studies of star formation in the EOG (Yasui et al. 2006, 2008), we explore in this paper the lifetime of circumstellar disks in a low-metallicity environment.

The frequency of disks harboring stars within a young embedded cluster, the disk fraction, has been studied for many clusters of various ages as an indicator of the disk lifetime (Haisch et al. 2001a; Hernández et al. 2007). The most common means of estimating the disk fraction is the detection of infrared emission from warm and hot dust (typically a few 100 to 1500 K) in the inner part of the disk (within a stellocentric distance of  $\sim 1$  AU) (Kenyon & Hartmann 1987) with wavelengths of 2–24  $\mu\text{m}$  using *K*-band (2.2  $\mu\text{m}$ ) (Lada 1999; Hillenbrand 2005), *L*-band (3.5  $\mu\text{m}$ ) (Haisch et al. 2001a), and *Spitzer IRAC* 3.6–8  $\mu\text{m}$  and/or *MIPS* 24  $\mu\text{m}$  (Sicilia-Aguilar et al. 2006) filters. The disk fraction was found to decrease as a function of age, showing that the inner disk lifetime is about 5–10 Myr for nearby embedded clusters with the solar metallicity. Because (sub-)mm continuum observations of cold dust ( $\sim 10$  K) in the outer disk ( $\geq 50$  AU) correlate very well with observations of inner dust disks (Andrews & Williams 2005), the entire disk, from 0.1 to 100 AU, is thought to be

---

<sup>1</sup>Based on data collected at Subaru Telescope, which is operated by the National Astronomical Observatory of Japan.

dispersed almost simultaneously (within  $\sim 10^5$  yr). Therefore, the lifetime of the entire disk is also thought to be 5–10 Myrs.

The disk lifetime in a low-metallicity environment is of special interest because of the discovery that the probability of a star hosting a planet increases with stellar metallicity (“planet-metallicity correlation”) (Gonzalez 1997; Fischer et al. 2005; Santos et al. 2003). However, the disk lifetime in an environment with lower metallicity than the solar neighborhood has not been studied. By directly studying the disk lifetime in the EOG, it may be possible to obtain clues to the mechanism of this “planet-metallicity correlation.” Although the disk fraction has been studied for a low-metallicity ( $[O/H] \simeq -0.5$ ) (Arnault et al. 1988) star-forming cluster, 30 Doradus, in the Large Magellanic Cloud (LMC) (Maercker & Burton 2005; Maercker et al. 2006), the target stars were limited to only very massive ones ( $\sim 20 M_\odot$ ) because of the limited sensitivity and spatial resolution for this extragalactic cluster. Because the EOG is much closer than nearby dwarf galaxies, it allows us to obtain accurate disk fractions in a low-metallicity environment to  $\sim 0.3 M_\odot$ , which is below the characteristic peak of IMF (Elmegreen et al. 2008). This mass detection limit corresponds to the lowest mass of the target stars for the planet-metallicity correlation (e.g., FGK-type stars) (Fischer et al. 2005) and is therefore critical for understanding the correlation.

## 2. OBSERVATION

Our targets, the Digel Cloud 2 clusters (Yasui et al. 2008; Kobayashi et al. 2008) are among the most distant embedded clusters in the EOG at  $R_g \sim 19$  kpc. They are located in a giant molecular cloud, Cloud 2, one of the most distant molecular clouds in the EOG (Digel et al. 1994). The metallicity  $[O/H]$  of Cloud 2 is measured at  $-0.7$  dex from the radio molecular emission lines (Lubowich et al. 2004), which is comparable to that of LMC ( $\sim -0.5$  dex) and Small Magellanic Cloud (SMC;  $\sim -0.9$  dex) (Arnault et al. 1988). The dust-to-gas ratio in Cloud 2 was estimated to be as low as 0.001 from a submm continuum observation (Ruffle et al. 2007). This is about 10 times smaller than in the solar neighborhood, and is consistent with the metallicity. Because the Cloud 2 clusters are much closer ( $D \simeq 12$  kpc) than LMC/SMC ( $D \sim 50$  kpc), they are quite suitable for the study of the disk fraction in a low-metallicity environment. Their youth (most likely age of  $\sim 0.5$  Myr) (Yasui et al. 2006, 2008; Kobayashi et al. 2008) adds an advantage to the present study because any variation in disk fraction should be most clearly seen when the disk fraction value is near its maximum. Because the EOG is located at the large heliocentric distance of  $\sim 10$  kpc, high sensitivity and high spatial resolution is necessary for the present study.

Deep  $JHK_S$ -band images of Cloud 2 clusters were obtained on September 2, 2006 with

an exposure time of  $\sim 600$  sec for each band with the 8.2-m Subaru telescope equipped with a wide-field NIR camera, MOIRCS (Ichikawa et al. 2006). The seeing was as good as  $\sim 0.35''$ – $0.45''$  through the night. As a result, we obtained deeper images than our preliminary studies of the Cloud 2 clusters (Yasui et al. 2006, 2008). All the data were reduced with IRAF<sup>2</sup> with standard procedures, and the results are shown in Fig. 1. *JHK* aperture photometry has been performed using IRAF apphot. The Mauna Kea Observatories (MKO) filters were used (Tokunaga et al. 2002). GSPC P330-E, which is a MKO standard (Leggett et al. 2006), was used for the photometric calibration. Because the fields of the Cloud 2 clusters are very crowded, we used the aperture diameters  $\sim 0.6''$  and  $0.5''$  for the Cloud 2-N and 2-S cluster members, respectively, to avoid the contamination of adjacent stars. The limiting magnitudes ( $10\sigma$ ) for the Cloud 2-N cluster are  $J = 22.3$  mag,  $H = 21.7$  mag,  $K_S = 21.2$  mag, while those for the Cloud 2-S clusters are  $J = 22.2$  mag,  $H = 21.3$  mag,  $K = 21.0$  mag. The achieved limiting magnitudes correspond to the mass detection limit of  $\sim 0.1 M_\odot$ , which is similar to the mass detection limit of extensive observations of embedded clusters in the solar neighborhood with smaller (2–4 m class) telescopes. Therefore, we can compare the disk fractions in the low-metallicity environment to those in the solar neighborhood on the same basis for the first time.

### 3. IDENTIFICATION OF CLUSTER MEMBERS

Because the Cloud 2 clusters are located behind the Cloud 2 molecular cloud (Yasui et al. 2006), the cluster members can be clearly identified as extinct red sources behind the CO dense cores on the sky (see Fig. 1; see also Fig. 1 in Kobayashi et al. 2008). We identified cluster members of the Cloud 2-N and 2-S clusters with the following criteria: (1) distributed in regions of the Cloud 2 clusters, which are defined by the yellow box and circle in Fig. 1, and (2) large  $A_V$  excess compared to normal field stars (extinction of  $A_V \geq 3.5$ ; see Fig. 2). On the color-magnitude diagram they are located in the region apart from the region of normal field stars because the Cloud 2 clusters are located at the peak of the Cloud 2 molecular cloud core (Kobayashi et al. 2008; Yasui et al. 2008) and reddened by the large extinction. We confirmed that stars with  $A_V \geq 3.5$  mag are concentrated on the cluster fields, while stars with  $A_V < 3.5$  mag are widely distributed over the observed field. In Fig. 2 the identified cluster members in the cluster regions are shown with red circles while all the sources outside the cluster regions ( $\sim 3.5' \times 4'$  region around each cluster) are shown with

---

<sup>2</sup>IRAF is distributed by the National Optical Astronomy Observatories, which are operated by the Association of Universities for Research in Astronomy, Inc., under cooperative agreement with the National Science Foundation.

black dots. As a result, we identified 52 and 59 cluster members for the Cloud 2-N and 2-S clusters, respectively, with the  $10\sigma$  limiting magnitude (red circles in Fig. 2) in both  $K_S$  and  $H$  bands.

Considering the very large  $R_g$  of the Cloud 2 clusters ( $R_g \simeq 19$  kpc), contamination of background stars is negligible and most of the field objects are foreground stars (some are background galaxies). To quantify the contamination by foreground stars, we compared the  $A_V$  distributions of all the sources in the cluster regions and the field objects outside the cluster regions (Fig. 3). Because the number of field objects decreases significantly at  $A_V \sim 3.5$  mag, most cluster members can be distinguished from the field objects as red sources with  $A_V \geq 3.5$  mag. The contamination by the foreground stars are estimated by counting the field objects in the tail of the distribution at  $A_V \geq 3.5$  mag and divide it with the total number of the sources in the cluster regions:  $\sim 20\%$  and  $\sim 2\%$  for the Cloud 2-N and 2-S clusters, respectively. Note that the contamination is very small for the S cluster because of the smaller area of the cluster region. Although there must be some cluster members at  $A_V < 3.5$  that missed our identification, the number of such sources should not be significant in view of the geometry of the molecular clouds, which are in front of the clusters (Yasui et al. 2006, 2008).

#### 4. DISK FRACTION

We derived disk fractions of the Cloud 2 clusters using a  $J-H$  vs.  $H-K$  color-color diagram for the identified cluster members (Fig. 4). Stars with circumstellar dust disks are known to show a large  $H - K$  color excess (Lada & Adams 1992). On the  $JHK$  color-color diagram, stars without circumstellar disks are seen as main-sequence stars reddened with extinction, while stars with circumstellar disks are seen in “the disk excess region” (to the right of the dot-dashed line in (Fig. 4) because of thermal emission from hot dust disk with a temperature of 1000–1500 K. For the Cloud 2-N and 2-S clusters, the disk fractions are  $9 \pm 4\%$  (5/52) and  $27 \pm 7\%$  (16/59), respectively, where the ratio of stars with excess to the total number of stars is given in parentheses. The uncertainty of the disk fractions is estimated only from the Poisson errors because photometric errors are quite small with the median errors of 0.06 mag for  $(H - K)$  and  $(J - H)$  (Liu et al. 2003). Given the possible systematic uncertainty, we cannot say at this stage if the difference between the disk fractions of the Cloud 2-N and 2-S is significant. Because the above-discussed contamination from the foreground objects of  $A_V \geq 3.5$  mag may decrease the disk fraction, the actual disk fractions could be higher than the derived values here. However, the amount of the increase is estimated as  $+2.2\%$  and  $+0.5\%$  for the Cloud 2-N and -S clusters, respectively, when reducing the total number

of the identified cluster members (52 and 59 for the N and S clusters, respectively) by the estimated number of contaminated foreground objects ( $\sim 10$  and  $\sim 1$  for the N and S clusters, respectively). Because this maximum possible increase of the disk fraction is well within the large Poisson uncertainty (4 % and 7 % for the Cloud 2-N and 2-S clusters, respectively), we conclude that the effect of the background contamination on the disk fraction is small. In addition, in the case where we assume that all stars in the cluster regions are cluster members, the disk fractions for the Cloud 2-N and 2-S cluster become 6 % (5/89) and 21 % (16/78), respectively. Even in this extreme case, the amounts of the decrease ( $-3$  % for the Cloud 2-N cluster and  $-6$  % for the 2-S cluster) are again within the Poisson errors.

To confirm the negligible effect of the photometric errors, we estimated disk fractions of two extreme cases: one case is that  $(J-H)$  and  $(H-K)$  colors of all stars were systematically changed within the photometric uncertainties of each source to get the lowest disk fraction and the other case to get the highest disk fraction. Assuming a Gaussian distribution of the photometric errors, the probability that the color of a star is within the  $\pm 1\sigma$  offset is 68 % and the probability that the color of a star is redder than the  $1\sigma$  offset is about 16 % ( $= (100 - 68)/2$ ). Because the Cloud 2 clusters have about 50 members, the probability that *all* stars have redder colors than the  $1\sigma$  offset is  $0.16^{50}$ , which is essentially zero. If we assume that the probability distribution of disk fraction is Gaussian, the estimated disk fraction of the extreme case (probability  $0.16^{50}$ ) should have a probability less than the 3 sigma case (0.1 %). In the above extreme case (all the sources have  $+1\sigma$  or  $-1\sigma$  redder colors), we found that the disk fraction increases from 9 % to 19 % (N cluster) and from 27 % to 44 % (S cluster). Since such an extreme case only occurs with a probability of  $0.16^{50}$ , much less than a 3 sigma occurrence, we consider that the  $1\sigma$  photometric uncertainty must be much less than 3 % ( $((19 - 9)/3 \sim 3)$ ) and 6 % ( $((44 - 27)/3 \sim 6)$ ) for the Cloud 2-N and 2-S clusters, respectively, which is smaller than the Poisson errors.

In view of the low-metallicity environment of the EOG, there might be some fundamental differences between the clusters in the solar neighborhood and in the EOG, such as the reddening and the stellar mass distributions, that may require different treatments of the disk fraction estimation. In our earlier paper, we confirmed that the reddening vector as well as the main-sequence track on the color-color diagram does not change with metallicity down to the metallicity of the Cloud 2 (Yasui et al. 2008, section 4). Also, the stellar mass distributions of the Cloud clusters are suggested to follow the universal IMF, which is widely observed in the solar neighborhood (Yasui et al. 2006, 2008). Therefore, we conclude that the use of the same division of with/without disk as for the solar neighborhood is appropriate. As for the treatment of the different filter systems, see Yasui et al. (2008) for the detail.

## 5. *JHK* DISK FRACTION OF THE NEARBY EMBEDDED CLUSTERS

We derived the *JHK* disk fraction of various embedded clusters in the solar neighborhood using the photometry data in the literature (Table 1 and Fig. 5). We chose publications with the following criteria: i) *JHK* photometry data of cluster members are available in order to estimate disk fractions in the same way as for our data, ii) the mass detection limit is  $\leq 1 M_{\odot}$  (Haisch et al. 2001a), iii) all data in each embedded cluster are estimated in the same filter system. For all clusters we used the classical dwarf track in the Johnson-Glass system (Bessel & Brett 1988) and a reddening vector in the Arizona system (Rieke & Lebofsky 1985). *JHK* disk fractions were estimated in the same way as for the Cloud 2 clusters: the border line, which determines whether a star has a disk or doesn't have a disk, passes through the point of M6 type stars in the dwarf track on the color-color diagram.

Recent disk fraction studies often use *JHKL* data because thermal infrared ( $\lambda \geq 3 \mu\text{m}$ ) can trace the colder (thus, outer) disk, and disk fractions from *JHKL* data are thought to be a more robust signature of the circumstellar disk than those only from *JHK* data (Haisch et al. 2001a). However, disk fractions from only *JHK* data are about 0.6 of those from *JHKL* data with slightly more scatter on the disk fraction-age plot, and the estimated disk lifetime from *JHK* data is basically identical to that from *JHKL* data. Therefore, despite a little larger uncertainty, the disk fraction from only *JHK* data should still be effective even without thermal IR data. Since the detection sensitivity in the thermal infrared is still not enough for the distant clusters like those in the EOG, we can make use of the high detection sensitivity at *JHK* wavelengths to estimate the disk lifetime for the EOG clusters.

## 6. DISCUSSION

### 6.1. Disk Fraction in Low-metallicity Environment

We show the disk fractions of the Cloud 2 clusters, as well as of the derived disk fraction of seven embedded clusters in the solar neighborhood, in the disk fraction-age diagram (Fig. 5; see § 5). The disk fractions of the Cloud 2-N and 2-S clusters are significantly lower than nearby embedded clusters of similar age. As discussed in Section 4, the contamination from the foreground objects and the possible unidentified cluster members have only a small effect on the estimated disk fraction. Although the difference between the filter system for our data (MKO) and the data in the literature might cause some systematic offset for the disk fraction value, we confirmed that the disk fraction does not depend on the choice of the filter system by confirming that the disk fraction of a good reference cluster (NGC 2024



cluster) is identical for both CIT and MKO systems (see Appendix A).

Given the importance of the age of the clusters to the above conclusion, here we discuss the uncertainties of the age and the age spread of the clusters. Considering the IMF derived from  $K$ -band luminosity function (KLF), the age of the Cloud 2 clusters should be less than 2 Myr: the KLF fitting shows an unrealistic top-heavy IMF with the age of 2 Myr (Yasui et al. 2006, 2008). Therefore, we conservatively estimate that the age upper-limit of the Cloud 2 clusters is 1 Myr. Moreover, the suggested supernovae triggered star formation of the Cloud 2 clusters (Kobayashi et al. 2008) suggests the age of 0.4 Myr, which strongly supports the above estimate from the KLF. Because there is no spectroscopic study of the cluster members, there is no observed age spread information as for the nearby clusters as in e.g., Palla & Stahler (2000). Because the mean age of this cluster is estimated as  $\sim 0.5$  Myr, the age spread should be smaller down to  $\pm 0.5$  Myr as assumed in the young cluster model in Muench et al. (2000). Muench et al. (2002) estimated the age of the Trapezium cluster at  $0.8 \pm 0.6$  Myr. Palla & Stahler (2000) actually obtained smaller age spread for the youngest embedded clusters (rho Oph, ONC). Moreover, in the above triggered star formation picture (Kobayashi et al. 2008), the age spread of the Cloud 2 clusters should be small because of the single triggering mechanism at a certain time. Therefore, we conclude that the most likely age of the clusters is 0.5 Myr and no more than 1 Myr. Even if we consider the possible age range, the estimated disk fractions are still quite low compared with those in the solar neighborhood.

Although the Cloud 2 clusters appear to be quite close on the sky, they are totally independent clusters with a projected distance of  $\sim 25$  pc at the heliocentric distance of  $D \simeq 12$  kpc (Yasui et al. 2008). If they were located at the same heliocentric distance as the Orion dark cloud ( $D \simeq 400$  pc), the angular separation between the clusters becomes  $3.5^\circ$ , which is larger than  $2.5^\circ$  between two independent clusters, e.g., NGC 2024 and NGC 2071 clusters, listed in the previous study of  $JHK$  disk fraction (Lada 1999). Because the measured disk fractions for two *independent* clusters were similarly low, the disk fractions of embedded clusters in the low-metallicity environment are inferred to be universally low, at least in the EOG. In combination with the fact that *there are no very young ( $\leq 1$  Myr) embedded clusters of solar metallicity whose disk fractions are this low*, our results strongly suggest that disk fraction depends strongly on metallicity.

## 6.2. Why Lower Disk Fraction with Lower Metallicity?

The most simple interpretations of the low disk fraction are that the disk is optically thin either because of the collisional agglomeration of dust grains in the disk (Andrews & Williams



2005) or because of the low dust-to-gas ratio due to the low metallicity. However, the former is unlikely because the probability of dust collision, which is proportional to the square of dust density, should be rather low in the low-metallicity environment. The latter is also unlikely because the inner disk should be optically thick even with a metallicity of  $-1$  dex: opacity of the disk with the wavelength of  $2\,\mu\text{m}$  ( $\nu \simeq 1.5 \times 10^{14}$  [Hz]) at 0.1 AU is estimated to be  $\sim 10^5$ , assuming a minimum mass solar nebula (surface gas density of  $\simeq 5 \times 10^4$  g/cm<sup>2</sup> at 0.1 AU) (Hayashi 1981) and a standard power-law opacity coefficient  $\kappa_\nu$  ( $\simeq 15$ ;  $\kappa_\nu = 0.1(\nu/10^{12} \text{ [Hz]}) \text{ cm}^2 \text{ g}^{-1}$ ) (Beckwith et al. 1990), and considering the dust-to-gas ratio of 0.001 (Ruffle et al. 2007), which is 1/10 smaller than in the solar metallicity. If we assume that the typical disk-to-star mass ratio (0.01; e.g., Andrews & Williams 2005, Natta et al. 2006), we would expect the total disk mass of  $10^{-3} M_\odot$  for the lowest-mass stars in our sample ( $M_* \sim 0.1 M_\odot$ ). Because this is roughly one-tenth that of the minimum mass solar nebulae (0.01–0.02  $M_\odot$ ), we still expect a very large optical thickness of  $\sim 10^4$  at K-band, assuming that disk mass measured in the submm correlates directly with surface density in the inner regions. This assumption is used for disks in the solar metallicity environment (e.g., Andrews & Williams 2005). Even if we assume the lowest observed disk-to-star mass ratio in the nearby star forming regions ( $\sim 10^{-4}$ ; Andrews & Williams 2005), the expected optical thickness is still  $\sim 10^2$ . Model spectral energy distributions with various disk mass do not show a significantly different  $H - K$  color excess (less than 0.05 mag) even if the amount of dust disks decreased to 1/10 (Wood et al. 2002), which correspond to the dust-to-gas ratio of  $\sim 0.001$  in the EOG. Therefore, we conclude that the small disk fraction implies that the inner region of the disk is cleared out.

Note that optically thickness does not necessarily mean the existence of observable  $H - K$  excess for lowest-mass stars with low effective temperature ( $\sim 3000$  K) and with very low disk mass of  $10^{-3}$ – $10^{-8} M_\odot$  (e.g., Ercolano et al. 2009). Because the lowest mass stars of our samples ( $\sim 0.1 M_\odot$ ) are M6-type stars with an effective temperature ( $T_{\text{eff}}$ ) of  $\sim 3000$  K (see e.g., Fig. 7 bottom figure in Lada & Lada 2003), it may be inevitable that some lowest-mass stars in our sample do not have detectable  $H - K$  excess simply because of the less dust content under low-metallicity, thus contributing to the low disk fraction artificially. To investigate this effect, we made a plot of the disk fraction of the Cloud 2 clusters for all sources brighter than certain  $K$ -band magnitudes (Fig. 6). It is clearly seen that the disk fractions stay almost flat at the low level and do not *decrease* even including the M stars of the faintest magnitudes ( $K \sim 20$ ) that may lower the disk fraction as described above. Therefore, we conclude that the disk fraction is genuinely low for all sources down to the mass detection limit and that clearing out of the inner region of the disk is the reason for it. For the above arguments, we note two related studies. One is the detailed disk fraction study of the Trapezium cluster by Lada et al. (2004), who show that even for the latest M-type

stars (e.g., M9-type stars,  $\sim 0.02 M_{\odot}$ ,  $T_{\text{eff}} \sim 2600$  K at 1 Myr) has detectable  $H - K$  excess and the  $JHK$  disk fraction does not change even including the stars of this low-mass. In view of the youth of the Cloud 2 clusters ( $\sim 0.5$  Myr) that is similar to the Trapezium cluster, we would naively expect similar detectable K-band excess even for the lowest mass stars in our sample ( $\sim 0.1 M_{\odot}$ , M6-type stars) with  $T_{\text{eff}} \sim 3000$  K even with the low metallicity. Also, in the simulation by Wood et al. (2002), a detectable  $H - K$  excess is seen even with very small disk mass of  $10^{-6} M_{\odot}$  under solar metallicity (which corresponds to  $10^{-5} M_{\odot}$  with the metallicity of Cloud2), assuming a central source with  $0.6 M_{\odot}$  and  $T_{\text{eff}} = 4000$  K.

Why does the inner region of the disk becomes cleared out effectively with lower metallicity? There are two well-known mechanisms that can clear the inner disk: dust sublimation (Millan-Gabet et al. 2007) and the X-wind model (Shu et al. 1994). In the following, we discuss if these mechanisms can effectively work with lower metallicity. *i) Dust sublimation:* Since dust sublimation typically occurs around 1500 K, the very inner part of the disk with  $T > 1500$  K becomes dust-free. The dust sublimation radius,  $R_s$ , is described approximately as  $(L_*/4\pi T_{\text{rim}}^4 \sigma)^{1/2}$ , where  $L_*$  is stellar luminosity,  $T_{\text{rim}}$  ( $\sim 1500$  K) is disk temperature at inner disk radius ( $R_s$ ), and  $\sigma$  is the Stefan-Boltzmann constant (Dullemond et al. 2007). However, because the inner disk is expected to be optically thick even with the low metallicity of  $-1$  dex, the temperature distribution inside the disk for  $-1$  dex should not differ from that for the solar metallicity (0 dex). Therefore,  $R_s$  is not expected to be significantly larger in the lower-metallicity environment. *ii) X-wind model:* Due to the interaction between the stellar magnetic field with the accretion disk, the gas disk is thought to be truncated at an inner radius of  $R_x = \Phi_{\text{dx}}^{-4/7} (\mu_*^4 / GM_* \dot{M}_D)^{1/7}$  (Shu et al. 2000), where  $M_*$  is the star's mass,  $\dot{M}_D$  is the disk accretion rate,  $\mu_*$  is magnetic dipole moment,  $\Phi_{\text{dx}}$  is a dimensionless number of order unity, and  $G$  is the gravitational constant. Among these parameters determining  $R_x$ , only the disk accretion rate,  $\dot{M}_D$  depends on metallicity. The magnetorotational instability (MRI), which is the most likely cause for disk accretion (Hartmann 2009), largely depends on the ionization of the gas disk by Galactic cosmic rays (Gammie 1996), X-rays from the central young star (Igea & Glassgold 1999), and thermal ionization (Sano et al. 2000). In a low-metallicity environment, we can expect that the ionization fraction increases and that the dead zone, which is the MRI inactive region of the disk (Gammie 1996), shrinks because the recombination on grain surfaces is reduced. As a result,  $\dot{M}_D$  increases and  $R_x$  decreases. In fact, Sano et al. (2000) suggested that the dead zone shrinks in the case that the dust sedimentation of dust grain proceeds, which mimics the case in the low-metallicity. On the other hand, low-metallicity also means fewer molecular ions, which would reduce the ionization fraction (e.g., Sano et al. 2000), and thus would reduce  $\dot{M}_D$ . Which process dominates in the low metallicity environment has not been determined conclusively since the combination of many physical processes determine the size of the dead zone (e.g, Fromang,

Terquem, & Balbus 2002). However, the former process, thus larger  $\dot{M}_D$ , may dominate (T. Sano, T. Suzuki, F. Shu, private communication).

Although further theoretical studies are necessary to have a firm conclusion, we would naively expect that  $R_x$  is not significantly larger in a lower-metallicity environment, and it appears that there is no theoretical reason to suspect that lower metallicity would make disks less detectable through the H-K excess. The lower dust level would still result in an optically thick inner edge and the size of the cleared out inner region should not change significantly with the metallicity. Therefore, our observations can simply be interpreted that the inner disk (gas and dust) is mostly absent in Cloud 2-N and 2-S.

### 6.3. Short Disk Lifetime in a Low-metallicity Environment

The above arguments lead to the suggestion that *the initial disk fraction (age = 0 in Fig. 5) in the low-metallicity environment of our targets is expected to be as high as that for the solar metallicity case*, assuming that the distribution of initial disk properties is exactly the same regardless of metallicity. Although this assumption is not obvious and more detailed observations of the disks in the extreme outer Galaxy are needed, it is not an unreasonable assumption because the star formation process from gas to stars do not seem to significantly change for the metallicity of the Cloud 2 clusters, for example, in view of the universal IMF throughout various physical/chemical environments (e.g., Elmegreen et al. 2008, see Omukai et al. 2000 for theoretical study). Therefore, we suggest that the significant decrease of the disk fraction in Fig. 5 is a result of the much shorter lifetime ( $\sim 1$  Myr) of the inner disk in the low-metallicity environment compared to that in the solar metallicity environment, 5–6 Myr from *JHK* disk fraction (§ 5, Lada 1999). This can be expressed with the rapid decrease of the disk fraction as shown with the red thick line in Fig. 5.

We know that the entire circumstellar disk, both the inner and outer disks, dissipates almost simultaneously in the solar metallicity environment because the submillimeter detection fraction and the fraction of objects with a NIR excess are identical (Andrews & Williams 2005), and also because the observed fraction of transition objects, between the Class II and Class III states, is very low (Duvert et al. 2000). Therefore, we suggest that the *entire* disk dispersal is also rapid in the low-metallicity environment. The distributions of  $(H-K)$  excess in the Cloud 2 clusters, which are consistent with those of more evolved ( $\sim 5$  Myr) embedded clusters with solar metallicity, also support the above idea, though other mechanisms might cause the formation of the similar  $(H-K)$  distributions. We constructed intrinsic  $H-K$  color distributions (Fig. 7) for Cloud 2 clusters and nearby embedded clusters (Table 1). The intrinsic  $(H-K)$  colors of each star were estimated by dereddening along the reddening

vector to the young star locus in the color-color diagram (see Fig. 4). For convenience the young star locus was approximated by the extension of the CTTS locus (gray lines in Fig. 4), and only stars that are above the CTTS locus were used. For the Cloud 2 clusters (Fig. 7, top), the CTTS locus in the MKO system (Yasui et al. 2008) was used, while for the nearby clusters (Fig. 7, bottom), the original CTTS locus in the CIT system (Meyer et al. 1997) was used. To make the figure clearer, we show the color distributions for only NGC 2024 (Haisch et al. 2000), Taurus (Kenyon & Hartmann 1995), and IC 348 (Haisch et al. 2001b), which have significantly different disk fractions. It is clearly seen that the distribution becomes bluer and sharper with lower disk fractions. The distributions of the Cloud 2 clusters resemble that of IC 348, whose disk fraction is as low as the Cloud 2 clusters ( $\sim 20\%$ ).

#### 6.4. Physical Mechanism for the Rapid Disk Dispersal in a Low-metallicity Environment

As the mechanism of disk dispersal, two possibilities are known : (i) disk accretion (Hartmann et al. 1998), and (ii) photoevaporation of the surface layer of the gas disk due to extreme-ultraviolet (EUV) radiation from the central star and/or the external radiation field (Hollenbach et al. 2000). In the low metallicity environment, both possibilities may work effectively. First, the disk accretion rate may increase in the low-metallicity as discussed in § 6.2, if the increase of the ionization fraction due to less dust is larger than the decrease of the ionization fraction due to less molecular ions. This could be the reason for the rapid disk dispersal. Secondly, the photoevaporation process may also work effectively to shorten the disk lifetime. Because the EUV photoevaporation is solely based on the Strömgren condition of the hydrogen gas, metallicity (or dust-to-gas ratio) should not affect the rate of the photoevaporation mass-loss. However, the recent theoretical work (Gorti & Hollenbach 2009) shows that far-ultraviolet (FUV) or X-ray radiation is more effective than EUV to photoevaporate the disk. Because FUV penetration strongly depends on the amount of dust in the disk, they found that the disk lifetime decreases with the dust opacity. Although the dust opacity dependence of the disk lifetime is not strong (factor of  $\sim 2$  changes with the dust opacity change of 10), they noted that the results are still in a preliminary stage and has to wait further detailed modeling. Therefore, this could be also the reason for the rapid disk dispersal in low-metallicity. In addition, something specific to the EOG environment might be the reason (see e.g., Haywood 2008), but obviously further studies are necessary to pin down the physics of this phenomena.

### 6.5. Implication to the Planet-metallicity Correlation

If the lifetimes of disks at the solar metallicity ( $[\text{O}/\text{H}] \sim 0$ ) and at the low-metallicity ( $[\text{O}/\text{H}] \sim -0.7$ ) are approximated as 5 Myr and 1 Myr, respectively, our results suggest that the disk lifetime strongly depends on the metallicity ( $Z \equiv [\text{M}/\text{H}]$ ) with a  $\sim 10^Z$  dependence. Because the disk lifetime ( $\tau_{\text{disk}}$ ) is directly connected to the planet formation probability ( $p_{\text{pl}}$ ), the strong metallicity dependence of  $\tau_{\text{disk}}$  may create a similarly strong metallicity dependence of  $p_{\text{pl}}$ . Therefore, the disk dispersal could be one of the major driving mechanisms for the planet-metallicity correlation, which shows a strong sharp ( $\sim 10^{2Z}$ ) metallicity dependence (Fischer et al. 2005). In the current standard core nucleated accretion model of the giant planet formation (e.g., see a review by Lissauer & Stevenson 2007), the planet formation time scale is determined both by the core growth time and the gas accretion time onto the core. Since the first study by Safronov (1969), core growth time in the giant planet zone has been thought to be far longer than the observed  $\tau_{\text{disk}}$ . But, after the discovery that  $\tau_{\text{disk}}$  is less than 10 Myr, it is widely accepted that giant planet cores must form via rapid runaway growth (Wetherill & Stewart 1989) and oligarchic growth (Kokubo & Ida 1998), which can grow the cores for the giant planet ( $5\text{--}10 M_{\oplus}$ ) at the outer disk (5 AU) in a reasonable time, e.g, 10 Myr. Because this growth time is comparable to  $\tau_{\text{disk}}$ , the variation of  $\tau_{\text{disk}}$  due to the metallicity around this timescale may cause a strong metallicity dependence of the planet formation probability,  $P_{\text{pl}}$ , thus contributing to the planet-metallicity correlation.

As far as we know, a deterministic model based on the core-accretion model by Ida & Lin (2004) is the only study that quantitatively estimates the effect of  $\tau_{\text{disk}}$  variation on  $P_{\text{pl}}$ . They show that the planet formation probability decreases with decreasing  $\tau_{\text{disk}}$  (see their Fig.2 (b)). However, the amount of decrease is only a factor of 2–4 with a factor of 10 change in the disk lifetime: the dependence is more like  $P_{\text{pl}} \sim \tau_{\text{disk}}^{0.5}$  and is not a strong function of  $\tau_{\text{disk}}$ . If this is the case, our suggestion that  $\tau_{\text{disk}} \sim 10^Z$  means the disk dispersal can contribute to the planet-metallicity correlation by a factor of  $10^{0.5Z}$ . Ida & Lin (2004) show that the core-accretion model can qualitatively explain the planet-metallicity relation, but also note that the suggested metallicity dependence is not as strong as the observed relation: it is more like  $\sim 10^Z$  dependence judging from their Fig. 2 (b). Therefore, by adding the contribution from the disk dispersal ( $\sim 10^{0.5Z}$ ), most of the observed metallicity dependence of the planet formation probability ( $10^{2Z}$ ) can be reasonably explained. However, a quantitative argument is difficult at this stage because there are ambiguities and complexities in the planet formation models, and thus the planet-formation time scale. Note that other groups are trying to reproduce the steep metallicity dependence by introducing a critical solid mass (Wyatt et al. 2007; Matsuo et al. 2007) for the core accretion model.

While the planet-metallicity correlation appears to be clear in Fischer’s systematic work

(Fischer et al. 2005), Udry & Santos suggest that the correlation in low-metallicity range ( $[\text{Fe}/\text{H}] < 0$ ) may be relatively weak (Udry & Santos 2007). Santos suggests that the planet formation mechanism could be different for the two metallicity ranges: core-accretion for the high-metallicity range and disk instability for the low-metallicity range (Santos 2008). Because our results seem to qualitatively explain a significant part of the  $10^{2Z}$  dependence of the planet-metallicity relation, we assume that the dependence also holds true in the low-metallicity range ( $[\text{Fe}/\text{H}] < 0$ ), where we made our observations. However, the core-accretion model may not be able to explain the existence of planets around the low-metallicity stars with such short disk lifetime.

## 7. Summary

We present deep imaging of two low-metallicity star forming regions in the EOG, Digel Cloud 2-N and Cloud 2-S.

1. The fraction of young stars with disks is found to be  $9 \pm 4\%$  for Cloud 2-N and  $27 \pm 7\%$  for Cloud 2-S. Previous works have shown that the age of these clusters is only approximately 0.5 Myr, and therefore the disk fraction is much lower than expected compared to the disk fraction measured for nearby star forming regions.
2. Various possibilities for the reason for the low disk fraction are investigated. We suggest that the simple reduction of the dust-to-gas ratio cannot explain the low disk fraction and that the initial disk fraction should be as high as in the solar neighborhood. We also suggest that dust sublimation and stellar magnetic activity cannot explain the enlargement of the inner disk hole in the low-metallicity environment. Therefore, the significant decrease of the disk fraction implies that the disk lifetime is much shorter ( $\sim 1$  Myr) than in the solar neighborhood (5–6 Myr). We suggest that the short disk lifetime is a result of the photoevaporation of the surface layer of the gas disk.
3. We suggest that the lower disk lifetime with lower metallicity may be a major factor in explaining the planet-metallicity correlation. But this is model-dependent and further theoretical and observational work is needed.

Although we derived disk fractions for two very young clusters in this paper, it is necessary to study more embedded clusters in the EOG to find a more quantitative relationship between the disk lifetime and the metallicity. It is also important to study the disks in longer wavelengths, e.g., *L*-band and mid-infrared wavelength, to confirm if disks at larger radii also



disappear rapidly, as suggested. These results will be a strong constraint for interpreting the planet-metallicity correlation, and ultimately for understanding how many planet-harboring stars we can expect in the Galaxy (Lineweaver et al. 2004).

C.Y has been supported by the Japan Society for the Promotion of Science (JSPS). We thank Dr. Ichi Tanaka for assistance with the observation and data reduction. We also thank Dr. Taku Takeuchi, Dr. Takeru Suzuki, Dr. Takayoshi Sano, and Dr. Frank Shu for helpful discussions on theoretical issues. We also thank the anonymous referee for the careful reading and thoughtful suggestions that improved this paper significantly.

### **A. Comparison of Disk Fractions in Different Filter Systems for the NGC 2024 Cluster**

NGC 2024 is a good reference target for the comparison of disk fractions in different filter systems because it is a very young (0.3 Myr) embedded cluster in the solar neighborhood (Meyer et al. 1997) with a high disk fraction (Lada 1999). The data were obtained on 1 January 2007 (based on data collected at the Subaru Telescope and obtained from the SMOKA, which is operated by the Astronomy Data Center, National Astronomical Observatory of Japan) with a field of view of  $\sim 3' \times 4'$  centered on  $(\alpha_{2000}, \beta_{2000}) = (05 : 41 : 41.4, -01 : 54 : 59.84)$ . The NGC 2024 data were reduced using the same procedures as the Cloud 2 data. For the photometry, we used only stars that are sufficiently isolated with an aperture radius of  $d = 3.4''$  ( $\sim 95\%$  energy). For the photometric calibration, we used five stars in the field, whose  $JHK$  photometric quality in 2MASS is good, after converting 2MASS magnitudes to MKO magnitudes.

Disk fractions can change in different mass ranges and in different spatial regions on the sky even when observed in the same filter system. The disk fraction estimated with stars, which are in the same region on the sky as the MOIRCS data and in almost the same mass range of  $\sim 0.7\text{--}0.02 M_{\odot}$  from a previous study in the CIT system (Levine et al. 2006), was  $55 \pm 17\%$  (10/18), which is consistent with the MOIRCS data ( $65 \pm 16\%$ , 17/26) within the errors. Moreover, almost all stars in the disk excess region in the CIT color-color diagram are located in the same excess region in the MKO color-color diagram. This is true also for the stars in the non-disk excess region. Therefore, we conclude that the disk fraction of NGC 2024 is correctly estimated in the MKO system.



## REFERENCES

- Andrews, S. M., & Williams, J. P. 2005, *ApJ*, 631, 1134
- Arnault, P., Knuth, D., Casoli, F., & Combes, F. 1988, *A&A*, 205, 41
- Balbus, S. A., & Hawley, J. F. 2000, *Space Science Reviews*, 92, 39
- Beckwith, S. V. W., Sargent, A. I., Chini, R. S., & Guesten, R. 1990, *AJ*, 99, 924
- Bensby, T., Feltzing, S., Lundström, I., & Ilyin, I. 2005, *A&A*, 433, 185
- Bessell, M. S. & Brett, J. M. 1988, *PASP*, 100 1134
- Bouvier, J., Alencar, S. H. P., Harries, T. J., Johns-Krull, C. M., & Romanova, M. M. 2007, *Protostars and Planets V*, 479
- Carpenter, J. M. 2001, *AJ*, 121, 2851
- D’Antona, F., & Mazzitelli, I. 1997, *Memorie della Societa Astronomica Italiana*, 68, 807
- D’Antona, F., & Mazzitelli, I. 1998, *ASP Conf. Ser. 134: Brown Dwarfs and Extrasolar Planets*, 134, 442
- Digel, S., de Geus E. J., & Thaddeus, P. 1994, *ApJ*, 422, 92.
- Dullemond, C. P., Hollenbach, D., Kamp, I., & D’Alessio, P. 2007, *Protostars and Planets V*, 555
- Duvert, G., Guilloteau, S., Ménard, F., Simon, M., & Dutrey, A. 2000, *A&A*, 355, 165
- Elmegreen, B. G., Klessen, R. S., & Wilson, C. D. 2008, *ApJ*, 681, 365
- Ercolano, B., Clarke, C. J., & Robitaille, T. P. 2009, *MNRAS*, 394, L141
- Ferguson, A. M. N., Gallagher, J. S., & Wyse, R. F. G. 1998, *AJ*, 116, 673
- Fischer, Debra A., & Valenti, Jeff. 2005. *ApJ*. 622. 110
- Fromang, S., Terquem, C., & Balbus, S. A. 2002, *MNRAS*, 329, 18
- Gammie, C. F. 1996, *ApJ*, 457, 355
- Gonzalez, G. 1997, *MNRAS*, 285, 403
- Gorti, U., & Hollenbach, D. 2009, *ApJ*, 690, 1539

- Haisch, K. E., Jr., Lada, E. A., & Lada, C. J. 2000, *AJ*, 120, 1396
- Haisch, K. E., Jr., Lada, E. A., & Lada, C. J. 2001a, *ApJ*, 553, L153
- Haisch, K. E., Jr., Lada, E. A., & Lada, C. J. 2001b, *AJ*, 121, 2065
- Hartmann, L., Calvet, N., Gullbring, E., & D’Alessio, P. 1998, *ApJ*, 495, 385
- Hartmann, L. 2009, *Accretion Processes in Star Formation*, 2nd edition, by Lee Hartmann. Cambridge, UK: Cambridge University Press, 2009. ISBN-13: 9780521531993,
- Hayashi, C. 1981, *Progress of Theoretical Physics Supplement*, 70, 35
- Haywood, M. 2008, *A&A*, 482, 673
- Hernández, J., et al. 2007, *ApJ*, 662, 1067
- Hillenbrand, L. A. 2005, *ArXiv Astrophysics e-prints*, arXiv:astro-ph/0511083
- Hollenbach, D. J., Yorke, H. W., & Johnstone, D. 2000, *Protostars and Planets IV*, 401
- Horner, D. J., Lada, E. A., & Lada, C. J. 1997, *AJ*, 113, 1788
- Ichikawa, T., et al. 2006, *Proc. SPIE*, 6269
- Ida, S., & Lin, D. N. C. 2004, *ApJ*, 616, 567
- Igea, J., & Glassgold, A. E. 1999, *ApJ*, 518, 848
- Kenyon, S. J., & Hartmann, L. 1987, *ApJ*, 323, 714
- Kenyon, S. J., & Hartmann, L. 1995, *ApJS*, 101, 117
- Kobayashi, N., Yasui, C., Tokunaga, A. T., & Saito, M. 2008, *ApJ*, 683, 178
- Kokubo, E., & Ida, S. 1998, *Icarus*, 131, 171
- Lada, C. J., & Adams, F. C. 1992, *ApJ*, 393, 278
- Lada, C. J., & Lada, E. A. 2003, *ARA&A*, 41, 57
- Lada, C. J., Muench, A. A., Lada, E. A., & Alves, J. F. 2004, *AJ*, 128, 1254
- Lada, C. J., Young, E. T., & Greene, T. P. 1993, *ApJ*, 408, 471
- Lada, E. A. 1999. Lada, C.J. & Kylafis, N.D. eds. 1999, *The Origin of Stars and Planetary Systems* pp. 441-78

- Leggett, S. K., et al. 2006, MNRAS, 373, 781
- Levine, J. L., Steinhauer, A., Elston, R. J., & Lada, E. A. 2006, ApJ, 646, 1215
- Lineweaver, C. H., Fenner, Y., & Gibson, B. K. 2004, Science, 303, 59
- Lissauer, J. J., & Stevenson, D. J. 2007, Protostars and Planets V, 591
- Liu, M. C., Najita, J., & Tokunaga, A. T. 2003, ApJ, 585, 372
- Lubowich, D. A., Brammer, G., Roberts, H., Millar, T. J., Henkel, C., & Pasachoff, J. M. 2004, in Origin and Evolution of the Elements, ed. A. McWilliam, & M. Rauch (Carnegie Observ. 4; Cambridge: Cambridge Univ. Press), 37
- Luhman, K. L. 2004, ApJ, 602, 816
- Maercker, M., & Burton, M. G. 2005, A&A, 438, 66
- Maercker, M., Burton, M. G., & Wright, C. M. 2006, A&A, 450, 253
- Matsuo, T., Shibai, H., Ootsubo, T., & Tamura, M. 2007, ApJ, 662, 1282
- Meyer, M. R., Calvet, N., & Hillenbrand, L. A. 1997, AJ, 114, 288
- Millan-Gabet, R., Malbet, F., Akeson, R., Leinert, C., Monnier, J., & Waters, R. 2007, Protostars and Planets V, 539
- Muench, A. A., Lada, E. A., Lada, C. J., & Alves, J. 2002, ApJ, 573, 366
- Natta, A., Testi, L., & Randich, S. 2006, A&A, 452, 245
- Omukai, K. 2000, ApJ, 534, 809
- Palla, F., & Stahler, S. W. 2000, ApJ, 540, 255
- Rebull, L. M., et al. 2002, AJ, 123, 1528
- Rieke, G. H., & Lebofsky, M. J. 1985, ApJ, 288, 618
- Rudolph, A. L., Fich, M., Bell, G. R., Norsen, T., Simpson, J. P., Haas, M. R., & Erickson, E. F. 2006, ApJS, 162, 346
- Ruffle, P. M. E., Millar, T. J., Roberts, H., Lubowich, D. A., Henkel, C., Pasachoff, J. M., & Brammer, G. 2007, ApJ, 671, 1766
- Safronov V. S. (1969) in 1972 English translation: NASA TTF-677, Nauka Press. Moscow.

- Sano, T., Miyama, S. M., Umebayashi, T., & Nakano, T. 2000, *ApJ*, 543, 486
- Santos, N. C., Israelian, G., Mayor, M., Rebolo, R., & Udry, S. 2003, *A&A*, 398, 363
- Santos, N. C. 2008, *New Astronomy Review*, 52, 154
- Shu, F., Najita, J., Ostriker, E., Wilkin, F., Ruden, S., & Lizano, S. 1994, *ApJ*, 429, 781
- Shu, F. H., Najita, J. R., Shang, H., & Li, Z.-Y. 2000, *Protostars and Planets IV*, 789
- Sicilia-Aguilar, A., Hartmann, L. W., Hernández, J., Briceño, C., & Calvet, N. 2005, *AJ*, 130, 188
- Sicilia-Aguilar, A., et al. 2006, *ApJ*, 638, 897
- Tokunaga, A. T., Simons, D. A., & Vacca, W. D. 2002, *PASP*, 114, 180
- Udry, S., & Santos, N. C. 2007, *ARA&A*, 45, 397
- Wetherill, G. W., & Stewart, G. R. 1989, *Icarus*, 77, 330
- Wood, K., Lada, C. J., Bjorkman, J. E., Kenyon, S. J., Whitney, B., & Wolff, M. J. 2002, *ApJ*, 567, 1183
- Wyatt, M. C., Clarke, C. J., & Greaves, J. S. 2007, *MNRAS*, 380, 1737
- Yasui, C., Kobayashi, N., Tokunaga, A. T., Terada, H., & Saito, M. 2006, *ApJ*, 649, 753
- Yasui, C., Kobayashi, N., Tokunaga, A. T., Terada, H., & Saito, M. 2008, *ApJ*, 674, 443

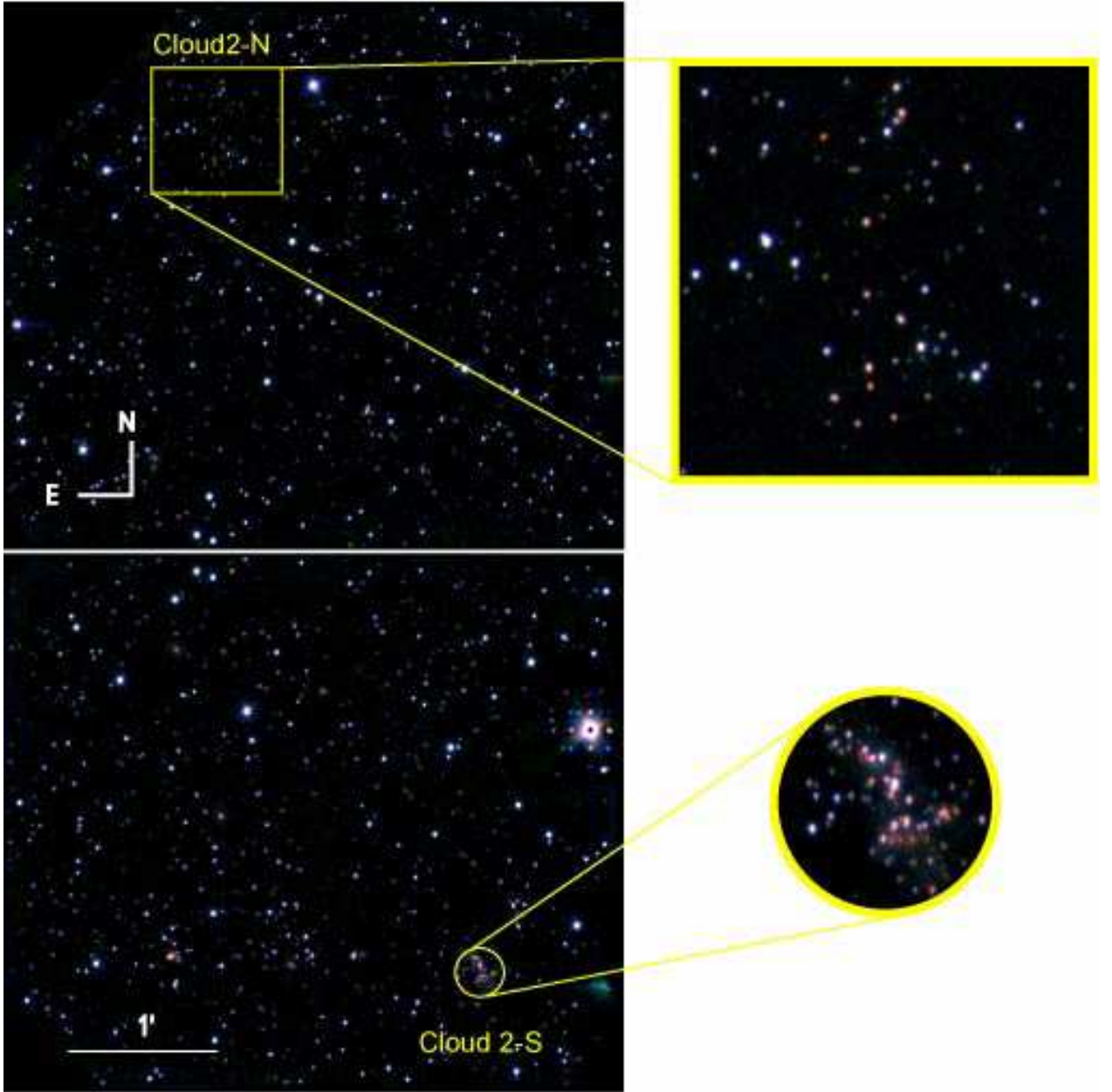


Fig. 1.— NIR pseudocolor images of the Cloud 2 clusters at the Galactic radius of  $R_g \sim 19$  kpc. The color images of Cloud 2-N (*top*) and 2-S clusters (*bottom*) are produced by combining the  $J$ - ( $1.26 \mu\text{m}$ ),  $H$ - ( $1.64 \mu\text{m}$ ), and  $K_S$ -band ( $2.14 \mu\text{m}$ ) images obtained at the Subaru telescope on September 2008. The field of view of both images is  $\sim 3.5' \times 4'$ . The yellow box and circle mark the locations of the clusters, with closeups shown on the right.

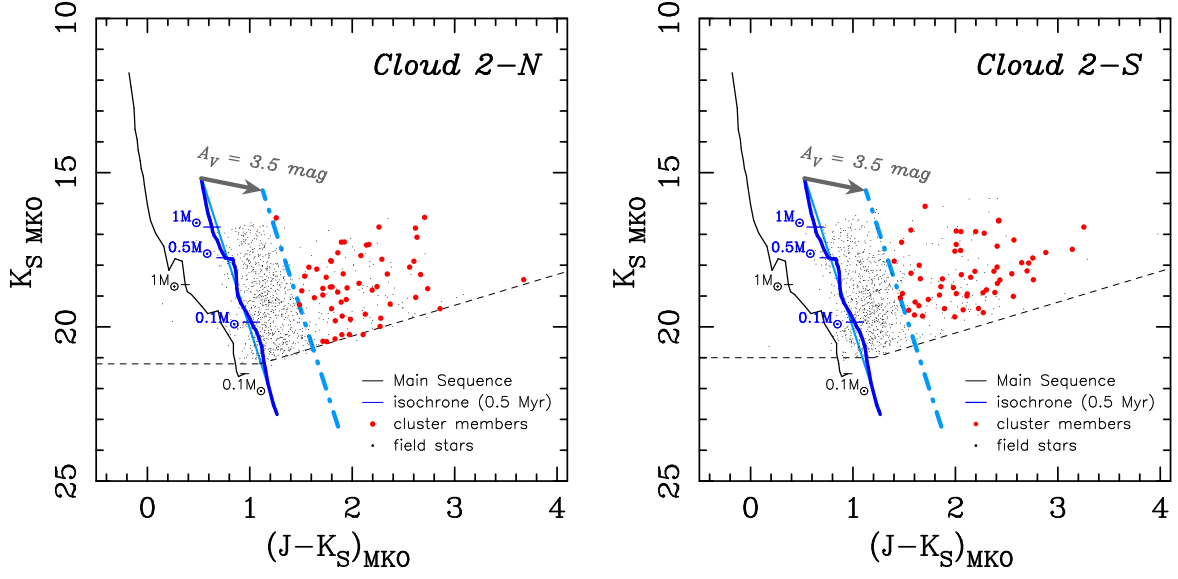


Fig. 2.—  $(J - K_S)$  vs.  $K_S$  color-magnitude diagrams (CMD) of the Cloud 2-N cluster (*left*) and the Cloud 2-S cluster (*right*). Identified cluster members in the cluster regions (yellow box and circle in Fig. 1) are shown with red circles while all the sources outside the cluster regions ( $\sim 3.5' \times 4'$  field for each cluster) are shown with black dots. Only stars detected with more than  $10\sigma$  in all  $JHK_S$  bands are plotted. The black lines show the dwarf tracks (Bessel & Brett 1988), while the blue lines show isochrone models (0.5 Myr, D'Antona & Mazzitelli 1997, 1998). For convenience, the isochrone model was approximated by the straight line shown with a solid aqua line. The gray arrows show the reddening vectors of  $A_V = 3.5$  mag from the isochrone model, while the dot-dashed aqua lines show the isochrone model with the extinction. Stars that are in the Cloud 2 clusters region on the sky and are located to the right of the dot-dashed lines on the CMD, are identified as the cluster members. The dashed lines show the limiting magnitudes ( $10\sigma$ ).

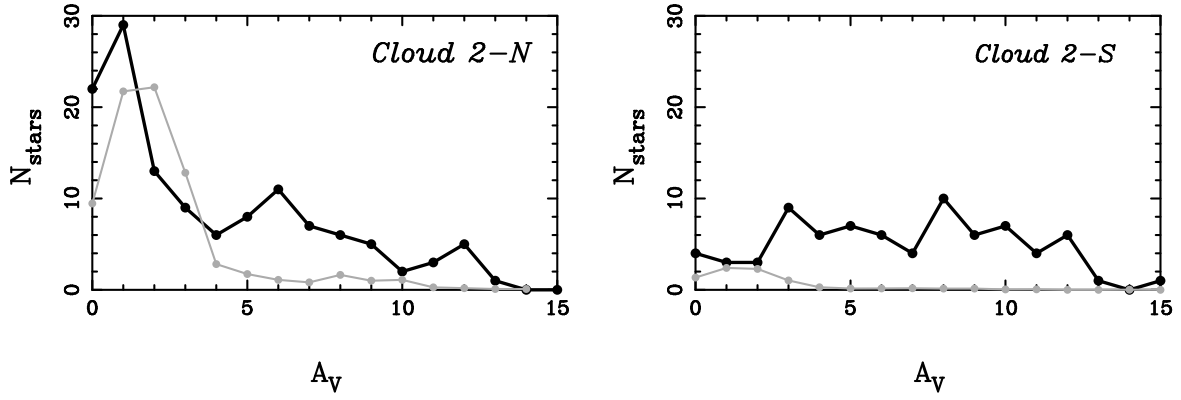


Fig. 3.—  $A_V$  distributions of all stars in the cluster region (cluster members; black dots and line) and all stars outside the cluster region (field objects; gray dots and line). The  $A_V$  is estimated from Fig 2 based on  $J - K$  colors. The distribution of field objects is normalized to match with the total area of the cluster regions. Because the number of field objects decreases significantly at  $A_V \gtrsim 3.5$  mag, most cluster members can be distinguished from the field objects as red sources with  $A_V \geq 3.5$  mag.



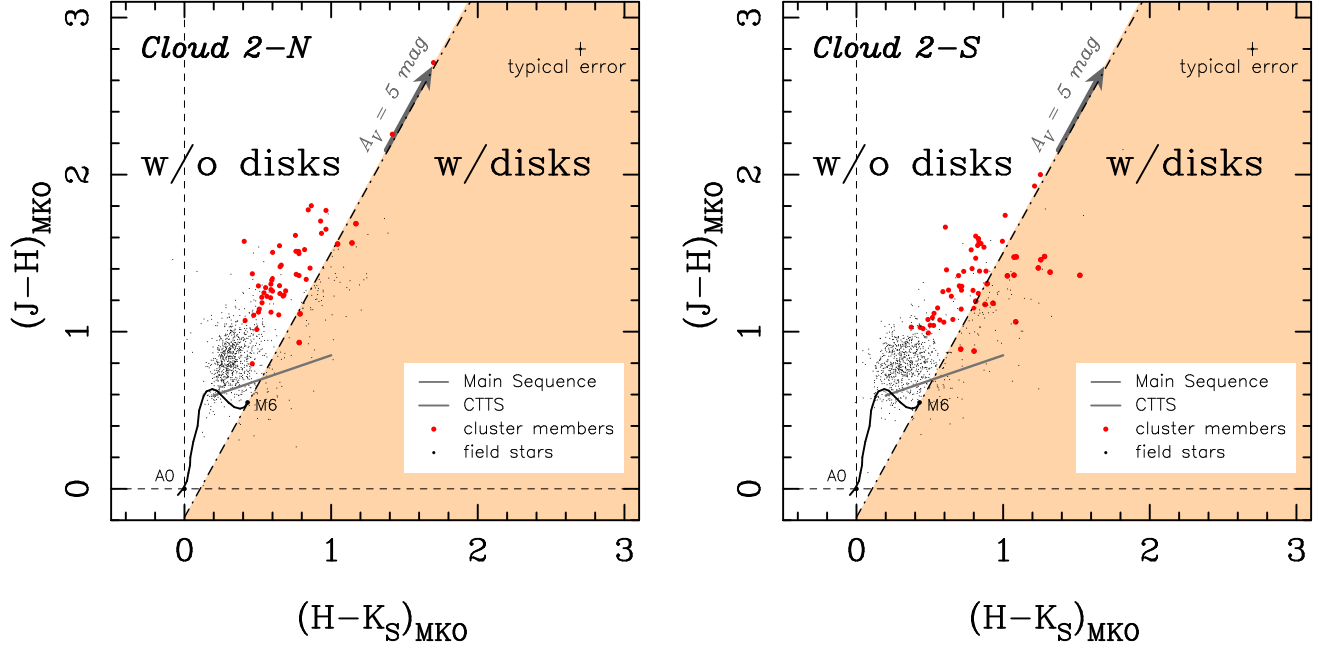


Fig. 4.—  $(J-H)$  vs.  $(H-K)$  color-color diagrams for the Cloud 2-N cluster (*left*) and the Cloud 2-S cluster (*right*) in the MKO system. Identified cluster members and field stars are shown with red filled circles and black dots, respectively. Typical uncertainty ( $1\sigma$ ) of the colors are shown at the top-right corner. The solid curve in the lower left portion of each diagram is the locus of points corresponding to the unreddened main-sequence stars. The dot-dashed line, which intersects the main-sequence curve at the maximum  $H-K_S$  values (M6 point on the curve) and is parallel to the reddening vector, is the border between stars with and without circumstellar disks. The classical T Tauri star (CTTS) loci are shown with gray lines.

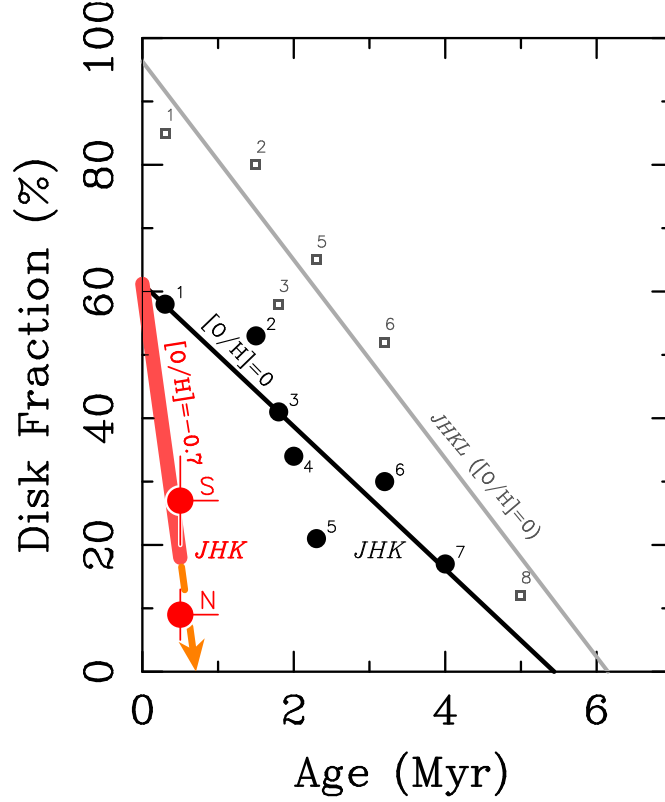


Fig. 5.— Disk fraction as a function of cluster age. *JHK* disk fractions of the Cloud 2 clusters are shown with red filled circles, while derived *JHK* disk fractions of other young embedded clusters with solar metallicity are shown with black filled circles (see § 5). The *JHKL* disk fractions of those other clusters (Haisch et al. 2001a) are shown with gray open squares. The black and gray lines show the disk fraction evolution under the solar metallicity, while the red line shows the proposed *JHK* disk fraction evolution in the low-metallicity environment. These lines are derived with least-squares fits.

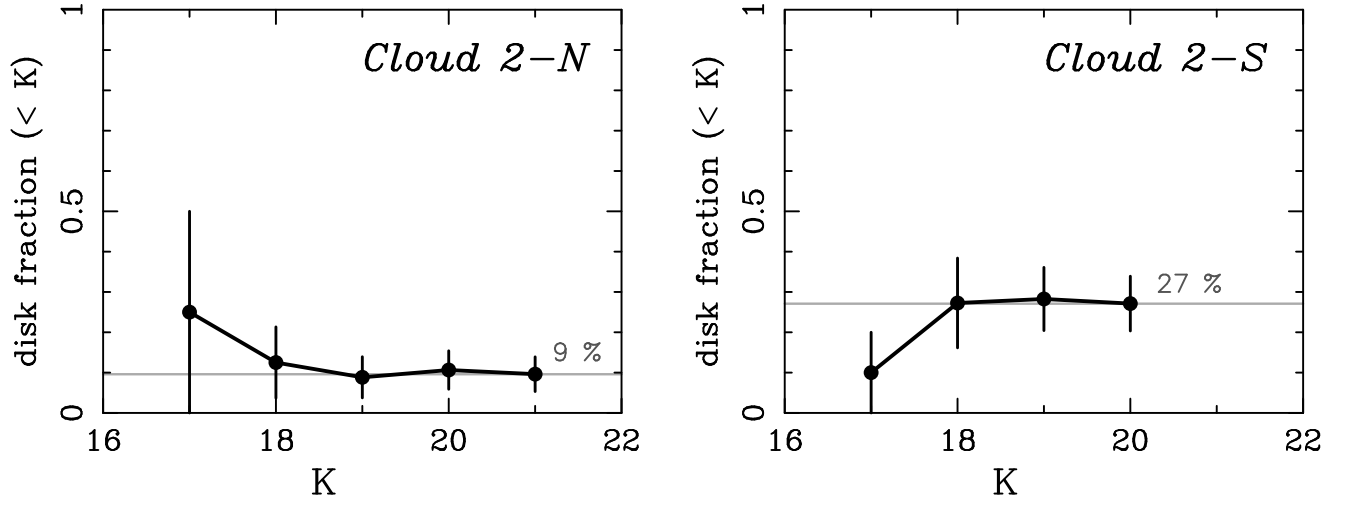


Fig. 6.— Disk fraction as a function of the  $K$ -band magnitude. Disk fractions are derived for all the sources brighter than the designated magnitude. It is clearly seen that the disk fractions stay almost flat at the low level and do not decrease within the uncertainty even including the late M stars at the faintest magnitudes ( $K \sim 20$ ).

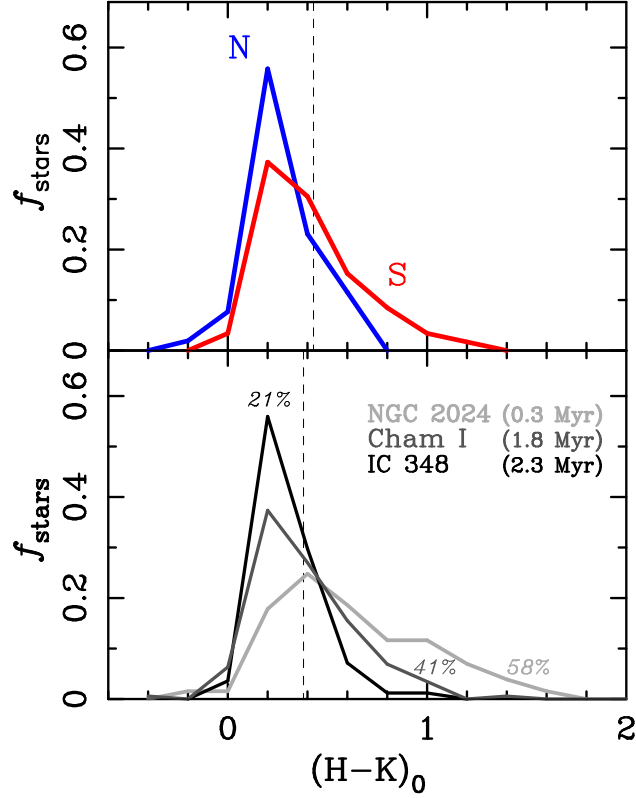


Fig. 7.— Comparison of intrinsic  $H - K$  color distributions. The fraction of stars ( $f_{\text{stars}}$ ) per each intrinsic color bin ( $(H - K)_0$ ) are plotted. *Top*:  $(H - K)_0$  distributions for the Cloud 2 clusters in the MKO system. *Bottom*:  $(H - K)_0$  distributions for the various young clusters in the solar neighborhood: NGC 2024 (Haisch et al. 2000), Cham I (Luhman 2004), IC 348 (Haisch et al. 2001b). Disk fractions of NGC 2024, Cham I, and IC 348 are 58 %, 41 %, and 21 %. The dashed lines show the borderlines for estimating the disk fraction. Note that the border of the  $(H - K)_0$  value for estimating the disk fraction (dashed line) differs slightly for different filter system.

Table 1: *JHK* disk fractions of embedded clusters in the solar neighborhood.

ID	Cluster	Age <sup>a</sup> (Myr)	<i>JHK</i> disk fraction (%)	Mass <sup>b</sup> ( $M_{\odot}$ )	Filter system <sup>c</sup>	Reference <sup>d</sup>
1	NGC 2024	0.3 (1)	$58 \pm 7$	0.13	SQUIID	2
2	Trapezium	1.5 (3)	$53 \pm 3$	$\sim 0.03$	SQUIID	4
3	Cham I	1.8 (3)	$41 \pm 4$	$\sim 0.03$	CIT	5
4	Taurus	2.3 (3)	$34 \pm 6$	0.3	SQUIID	6
5	IC 348	2.3 (3)	$21 \pm 4$	0.19	SQUIID	7
6	NGC 2264	3.3 (3)	$30 \pm 3$	$\sim 0.3$	SQUIID	8
7	Tr 37	4.0 (9)	$17 \pm 3$	$\sim 0.3$	2MASS	9

<sup>a</sup>References for the ages are shown in the parenthesis.

<sup>b</sup>Mass detection limit of the data.

<sup>c</sup>The photometric system of the *JHK* data obtained with the Simultaneous Quad Infrared Imaging Device (SQUIID) at Kitt Peak National Observatory is similar to the Johnson system and the CIT systems (Lada et al. 1993; Horner et al. 1997)

<sup>d</sup>References for the *JHK* photometric data. For Trapezium, only the Fred Lawrence Whipple Observatory (FLWO) data were used to match the mass detection limit (see Muench et al. 2002). A  $K_S$  filter was used instead of  $K$  filter for the observation of Tr 37.

References. — (1) Meyer et al. 1997; (2) Haisch et al. 2000; (3) Palla & Stahler 2000; (4) Muench et al. 2002; (5) Luhman 2004; (6) Kenyon & Hartmann 1995; (7) Haisch et al. 2001b; (8) Rebull et al. 2002; (9) Sicilia-Aguilar et al. 2005